The EuroBiotech Journal
RESEARCH ARTICLE
Medical Biotechnology

Electrode surfaces based on multiwall carbon nanotubes-chitosan composites validated in the detection of homocysteine biomarkers for cardiovascular disease risk monitoring

Suparerk Oonchit[1], Benya Cherdhirunkorn[1], Phuntila Tharabenjasin[2], Noel Pabalan[2], Kumpol Chintanavilas[2], Robert Marks[3], Yardnapar Parcharoen[2,4,*], Chiravoot Pechyen[1,4,*]

Abstract

This study aimed to modify screen-printed carbon micro-electrode surfaces by coating them with multiwall carbon-based nanotubes conjugated with chitosan and then validated the formed multiwall carbon-based nanotubes-chitosan coated screen printed carbon micro-electrode for the detection of homocysteine, a biomarker analyte known as a risk indicator in cardiovascular disease. The microstructure surface and crystallographic structure stability of the formed multiwall carbon-based nanotubes-chitosan obtained at formed multiwall carbon-based nanotubes per chitosan ratios of 1:1, 2:1, 3:1, and 4:1 were examined via field emission scanning electron microscopy, X-ray radiation, Raman spectroscopy, surface area and pore size, and thermogravimetric analyses. Homocysteine solutions at 30–100 μM were measured by cyclic voltammetry using the different formed multiwall carbon-based nanotubes-chitosan compositions as sensor electrodes. That with an optimal formed multiwall carbon-based nanotubes per chitosan ratio of 4:1 showed the highest crystallinity and electrical conductivity and gave a high coefficient of determination ($R^2 = 0.9036$) between the homocysteine concentration and the oxidation current detection over an operating range of 30–100 μM. This new composite microelectrode for detecting homocysteine concentration makes it a promising candidate for clinical applications.

Keywords: cardiovascular disease; sensor; homocysteine

Introduction

The world's aging population is projected to continue from 2015 to 2050 [1]. It is estimated that by 2040, the elderly population (aged 60 or older) in Thailand will have reached ~33% of the total population [2]. Older age increases the incidence of non-communicable diseases, including cardiovascular diseases (CVD), led by ischemic heart disease, coronary artery disease, and stroke [3].

Homocysteine (Hcy) is an amino acid produced when proteins are broken down. A high Hcy plasma level, also called hyperhomocysteinemia, can contribute to arterial damage and the formation of blood clots in the blood vessels. Elevated plasma Hcy concentrations or hyperhomocysteinemia (> 15 μM, which is typically used in extensive epidemiologic studies) due to a deficiency in the Hcy-metabolizing enzyme will promote atherosclerosis through increased oxidant stress, impaired endothelial function, and induction of thrombosis [4]. The formation of Hcy, a sulfhydryl containing amino acid, occurs as an intermediate during the metabolic conversion of methionine to cysteine [5]. Clinically, a high level of Hcy in the serum or urine is a likely biomarker of CVD risk [6, 7].

Regarding blood Hcy detection, high-performance liquid chromatography using fluorescence as a detector is a preferred method of its measurement [8, 9]. Alternatives, such as gas chromatography-mass spectrometry, chemiluminescence immunoassay, enzyme-linked immunoassay, and fluorescence polarization immunoassay, have sensitivities to detect Hcy at low concentrations [10]. Even though all these techniques have high sensitivity, they have the disadvantage of being costly lab-based methods. In con-

[1] Department of Materials and Textile Technology, Faculty of Science and Technology, Thammasat University, Khlong Luang, Pathum Thani 12120, Thailand.
[2] Chulabhorn International College of Medicine, Thammasat University, Khlong Luang, Pathum Thani 12120, Thailand
[3] The Avram and Stella Goldstein-Goren Department of Biotechnology Engineering, Ben-Gurion University of the Negev, Beer-Sheva, Israel
[4] Thammasat University Center of Excellence in Modern Technology and Advanced Manufacturing for Medical Innovation, Thammasat University, Patumthani 12120, Thailand.

***Corresponding authors:**
yardnapa@tu.ac.th and cpechyen@tu.ac.th

DOI: 10.2478/ebtj-2023-0010

© 2023 Authors. This work was licensed under the Creative Commons Attribution-NonCommercial-NoDerivs 4.0 License.

trast, medical services need a point-of-care diagnostic kit and necessitate using environmentally hazardous solvents, which we hope to address here.

More needs to be done regarding developing a Hcy biosensor [11]. Enzyme-based biosensors for detecting Hcy via cyclic voltammetry (CV) are rapid, highly sensitive, and low-cost; however, these methods are limited due to the overlap in the redox processes at a similar potential [12]. To help solve some of these issues, tailored microelectrodes [13-15] may provide a single-use, low-cost approach that enables design flexibility and potential for mass production [12, 16]. This is why one was developed for Hcy measurement as a warning biomarker for CVD in this study.

Little by way of Hcy biosensors exit [10, 17]. Those available were developed to screen for Hcy using a carbon paste electrode modified with multiwall carbon nanotubes (MWCNT) was prepared to study the electrocatalytic activity of dopamine (DP) and isoprenaline (ISP) in the presence of homocysteine (Hcy). It was used for the determination of Hcy. The peak current of oxidation of Hcy at MWCNT occurred at a potential of about 530 mV and 640 mV. The results showed that the oxidation peak current of Hcy at the modified carbon nanoelectrode was higher than on the not modified electrode. Still, these were tube limited in their measurement sensitivity of current val-ue. Thus, we solved this last issue by improving the electrode surface with multiwall carbon nanotubes (MWCNTs) since they exhibit high electrical conductivity, surface-to-area ratio, and strength. They, however, are highly hydrophobic, so they were encapsulated within chitosan (CS) to increase their hydrophilicity and conductivity.

Materials-Methods

The MWCNTs (diameter: 12 nm, length: 3–12 μm) with a purity of 99% were purchased from Nano Generation Co., LTD. The CS and L-Hcy (Sigma; CAS No. 6027-13-0) with a purity of 98% each and sodium dodecylbenzene sulfonate (NaDDBS; technical grade) were from Sigma-Aldrich (St. Louis, MO, USA). Glacial acetic acid with a purity of 99.8% was from RCI Labscan Limited, Thailand. Screen-printed carbon electrodes with carbon ink (SPCE; CI1703OR) were purchased from Quasense Co., Ltd. (Thailand) in the form shown in Figure 1.

2.1. Synthesis of MWCNTs-CS composites

This simple technique utilizes NaDDBS as a surface functionalizing agent for MWCNTs to provide a uniform, continuous, and well-defined mesoporous CS layer. For the MWCNTs solu-tions, 0.25, 0.5, 0.75, and 1 g of MWCNTs and 1% (w/v) NaDDBS in aqueous solution were mixed, and the suspension was vibrated by ultrasonication at 60 °C for two h. The CS solution was prepared by dissolving 0.2 g of CS in 3% (w/v) of glacial acetic acid and mixing by stirring at 40 °C for one hour. This was then combined with the MWCNTs at a MWCNTs: CS ratio of 1:1, 2:1, 3:1, and 4:1 in an ethanol solution of 0.5, 1, 1.5, and 2 mL, respectively, and stirred for two hours to achieve a uniform suspension. Next, a 30% (v/v) ammonia solution was added to the MWCNTs-CS to reach a pH of around 9–10, and then 3 mL of 99.9% ethanol solution was added and stirred for another 30 min. The suspension was then separated by centrifugation. The precipitate was washed with deionized water two or three times and dried. To

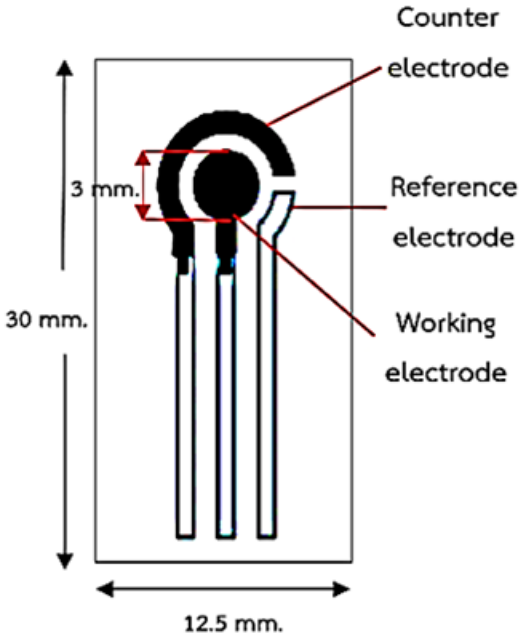


Figure 1. Schematic diagram showing the electrode configuration.

determine the crystal structure of the MWCNTs-CS, a sample was oven dried at 90 °C for 24 h.

2.2. Coating of the SPCEs with MWCNTs-CS

The dimensions of the electrode were 12.5 mm wide and 30 mm long. The working electrode and counter electrode were commercial SPCEs. The reference electrode was composed of a silver/silver chloride coating. The surface material was a plastic sheet. The diameter and area of the working electrode were 3 mm and 7.065 mm^2, respectively. The MWCNTs-CS composite solution was stirred for 30 min at room temperature before use for coating on the surface of the working SPCE (section 2.3). The configuration of the electrodes is shown in Figure 1.

2.3. Cyclic voltammetry (CV) of model analyte

The experiments were performed using the PSTrace software 5.9 instrument (PalmSens BV, Houten, Utrecht) using the three-microelectrodes device as fabricated in Section 2. A 0.5 µL MWCNTs-CS composite solution was deposited on the working electrode and dried at 50 °C for 10 min (or left at room temperature until dry).

The CV measurement was conducted over an electrode potential from -1.0 to 1.25 V at a scan rate of 0.1 V/s. Modified electrodes with while WCNTs-CS at different MWCNTS: CS ratios of 1:1, 2:1, 3:1, and 4:1 were used in this study. The bare electrode served as a control. To measure the Hcy concentration, a 0.5 µL solution at a Hcy concentration of 30, 60, or 100 µM was deposited onto the working electrode and scanned from -0.2 to 1.0 V at a scan rate of 0.1 V/s. The working electrode was stirred in pH 7.4 (PBS) phosphate buffer solution. The potential was held constant while additional Hcy was added to the PBS solution. After reaching equilibrium, the corresponding current was recorded.

2.4. Hybrid microelectrode characterizations

2.4.1. Field emission scanning electron microscopy (FE-SEM)

The microstructured surface of the MWCNTs-CS-coated surface was viewed under FE-SEM (JEOL JSM-7610F, Oxford X-Max 20) at a magnification of x50,000. Before testing, the sample was coated with gold and then measured at 5 kV with a sample size of 1 x 1 cm. The surface characteristics, including the size and shape of the particles, and phase dispersion, were recorded.

2.4.2. X-ray diffraction (XRD)

The crystal structures of the MWCNTs, CS, and MWCNTs-CS composites were prepared as powder form and assessed using powder XRD analysis (Bruker AXS Model D8 Advance, Germany). Diffraction patterns of the powdered samples were measured by CuKα radiation at a wavelength of 0.154 nm at 30 kV and 10 mA. The diffraction angle was examined over a 2θ range from 10–60 degrees. The XRD spectra indicate each substance's peak intensity and crystallinity and can be used for further reference in measuring analytical substances.

2.4.3. Raman spectroscopy

The molecular structures of the MWCNTs, CS, and MWCNTs-CS composites at different ratios were evaluated using Raman spectroscopy (Thermo Fisher Scientific DXR3 Raman Microscope, BEC Co., Ltd, Thailand) with an excitation laser wavelength at 532 nm, and grating at 900 lines/mm. The analysis is based on the principle of scattering light projected onto the specimen, which is prepared as a powder.

2.4.4. Brunauer-Emmett-Teller surface area (S_{BET}) and pore size analyses

The surface area, pore volume [determined from a relative pressure (P/Po) of 0.99], and average pore diameter [calculated using the density functional theory (DFT) method] measurements were examined by the BET method using nitrogen (N_2) adsorption at 77 K.

2.4.5. Thermogravimetric analysis (TGA)

The TGA, which measures the weight change of a substance based on its thermal stability properties, was performed using a TGA 2 (Mettler Toledo, Switzerland) instrument. The MWCNTs, CS, and MWCNTs-CS composites at different ratios were analyzed over a TGA tem-perature range from 30 °C to 600 °C under atmospheric nitrogen at 20 mL/min flow and a heating rate of 10 °C/min.

2.4.6. Electrochemical properties

The Hcy testing was analyzed by PalmSens BV analyzers equipped with the PSTrace software version 5.9. Using varied ratios of MWCNTs-CS composites, increased hybrid microelectrode conductivity was compared to bare electrode conductivity by CV.

Results

3.1. FESEM

To investigate the topographical and elemental information of the MWCNTs, CS, and MWCNTs-CS formed at different MWCNTs: CS ratios and to confirm the adhesion of CS on the surface of MWCNTs, the images of all composites were examined under FE-SEM at a magnification of x50,000. The MWCNTs were found to be nested as longitudinal filaments (Figure 2a), while CS showed a large adhesion plate, non-porous, and smooth tissue (Figure 2b). The diameter of the MWCNTs-CS was ≈40-50 nm and CS was clustered on the surface of the MWCNTs formed at all composite ratios, indicating a pronounced adhesion between them (Figure 2c-f). However, a high proportion of CS could impede the generation of an electrical current from the MWCNTs. Our results showed that the MWCNTs-CS formed at a MWCNTs-CS ratio of 4:1 gave an excellent organization of MWCNTs-CS (Figure 2f). Therefore, the electrochemical properties of MWCNTs-CS formed at a MWCNTs: CS ratio of 4:1 was further examined.

3.2. Evaluation of the crystallographic structure by XRD analysis

To determine the crystallographic structure of MWCNTs, CS,

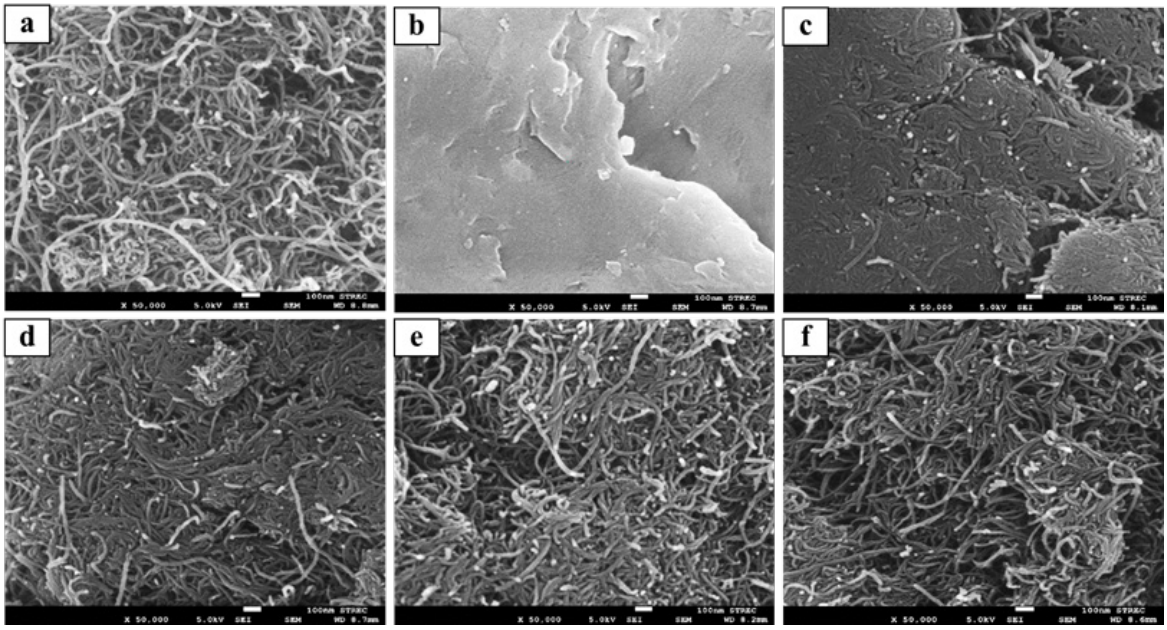


Figure 2. Representative FE-SEM images of MWCNTs-CS composites formed at different MWCNTs: CS ratios, showing (a) MWCNTs, (b) CS, and (c–f) MWCNTs-CS formed at MWCNTs: CS ratios of (c) 1:1, (d) 2:1, (e) 3:1, and (f) 4:1, respectively, (x 50,000 magnification).

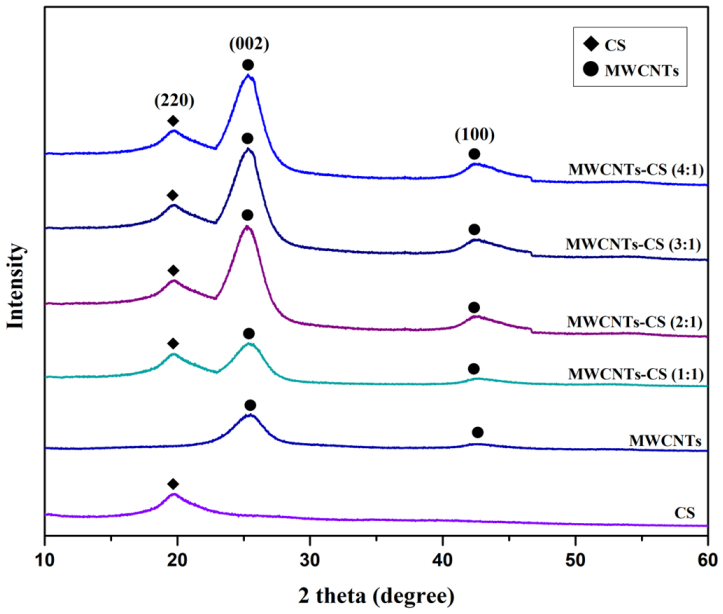


Figure 3. Representative XRD patterns of the CS, MWCNTs, and MWCNTs-CS composites at different ratios.

MWCNTs-CS (1:1), MWCNTs-CS (2:1), MWCNTs-CS (3:1), and MWCNTs-CS (4:1) samples were exposed to powder XRD radiation spectrophotometer using a CuKα light source (Figure 3). As expected, MWCNTs-CS (1:1), MWCNTs-CS (2:1), MWCNTs-CS (3:1), and MWCNTs-CS (4:1) showed the highest crystallization at a 2θ of 19.7°, 25.2°, and 42.7°. The XRD pattern showed the pure hexagonal phase of MWCNTs as the appearance of intense peaks at a 2θ of 25.5° and 42.7° with an index of (002) and (100) reflections, respectively, [18]. The XRD pattern showed the phase of pure CS intense peaks at a 2θ of 19.7° with an index to the (220) reflections. The broadening of the CS peaks is due to the amorphous nature of the polymer [19]. In this XRD pattern, no peak impurities were observed. The MWCNTs-CS composites peak at 25.2° had a reasonably high crystallinity and pronounced width range. The lowest physical stability was observed in CS, as represented by the lowest peak intensity. For CS, the 2θ ranged from 19.8–20.7°, in accordance with a previous study [20].

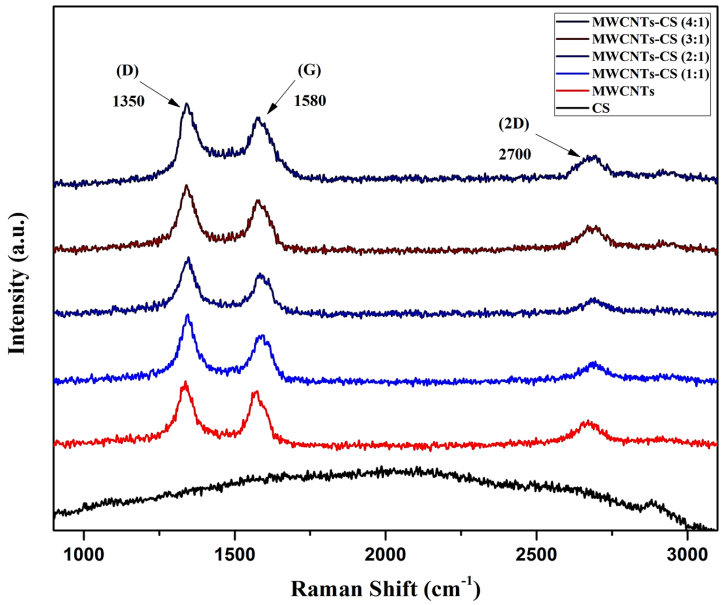


Figure 4. Raman patterns of CS, MWCNTs, and MWCNTs-CS composites at different ratios.

3.3. Raman spectroscopy analysis

The molecular structure was analyzed using Raman spectroscopy to determine the substances configuration, purity, and crystallinity. The Raman spectra of MWCNTs, MWCNTs-CS (1:1), MWCNTs-CS (2:1), MWCNTs-CS (3:1), and MWCNTs-CS (4:1) are shown in Figure 4 over a wavelength range of 900–3100 cm^{-1}. The spectra exhibited the elongation of the C-C bond in the graphite material, resulting in a property known as the G-band, which shows sp^2 hybridization. The G band represented the strain from the skeletal stretching vibration mode of the MWCNTs component and was seen at approximately 1580 cm^{-1}. The observed D band at 1350 cm^{-1} is due to the disorder of the carbon structure, the degree of graphitization of the G band, and phonon resonance of the G' band, which showed a 2D signal at 2700 cm^{-1} [18, 21]. For CS, the Raman spectrum of pure CS does not exhibit clear bands in the visible region. Still, when CS interacts with MWCNTs, the peaks of MWCNTs are shifted to higher wavelengths, showing a strong relationship between the MWCNTs and CS. This is due to the increased energy of the CS-coated MWCNTs [22]. The hydrophobic and π–π interactions between the CS ($-C=OCH_3$) and (C=C) bands have an increased vibrational energy, and so a shift in the Raman signal bands is seen [23]. The recorded Raman spectra demonstrate that forming MWCNTs-CS composites is possible in CS. Therefore, an investigation of the molecular structure of MWCNTs-CS composites was performed to confirm the strength and increased energy of the structure for the measurement of its electrochemical properties.

3.4. Surface area and pore size analysis

To investigate the porosity types (e.g., microporous and mesoporous) of the CS, MWCNTs, MWCNTs-CS (1:1), MWCNTs-CS (2:1), MWCNTs-CS (3:1), and MWCNTs-CS (4:1), N_2 adsorption/desorption isotherms were examined by BET measurements. The isotherms for the MWCNTs present type I characteristics, based on the international union of pure and applied chemistry (IUPAC), indicating the presence of microporous pores (pore width ≈ 2 nm) at relatively low pressures ($P/P_0 < 0.1$). In contrast, the isotherms for the MWCNTs-CS exhibit combined characteristics of types I/

Table 1. The pore properties of CS, MWCNTs, and MWCNTs-CS composites at different ratios.

Samples	BET surface area (m^2/g)	Pore volume (cc/g)	Pore size (nm)
Chitosan (CS)	99	1.04	149.5
MWCNTs	416	2.82	12.3
MWCNTs-CS (1:1)	219	1.41	27.1
MWCNTs-CS (2:1)	233	1.56	23.4
MWCNTs-CS (3:1)	320	1.75	18.8
MWCNTs-CS (4:1)	384	2.06	18.2

IV, indicating the presence of mesoporous pores (pore width 2–50 nm, IUPAC) classification at an intermediate relative pressure ($P/P_0 \approx 0.4$). Detailed information of the specific surface areas, pore volumes, average pore diameters, and pore volume fractions for the CS, MWCNTs, MWCNTs-CS (1:1), MWCNTs-CS (2:1), MWCNTs-CS (3:1), and MWCNTs-CS (4:1), is summarized in Table 1. As outlined in Table 1, the specific surface area for the two types of porous MWCNTs-CS was increased compared to the single phase of CS. The volume fraction of the MWCNTs-CS (1:1), MWCNTs-CS (2:1), MWCNTs-CS (3:1), and MWCNTs-CS (4:1) was significantly (and numerically much) higher than those of the CS without

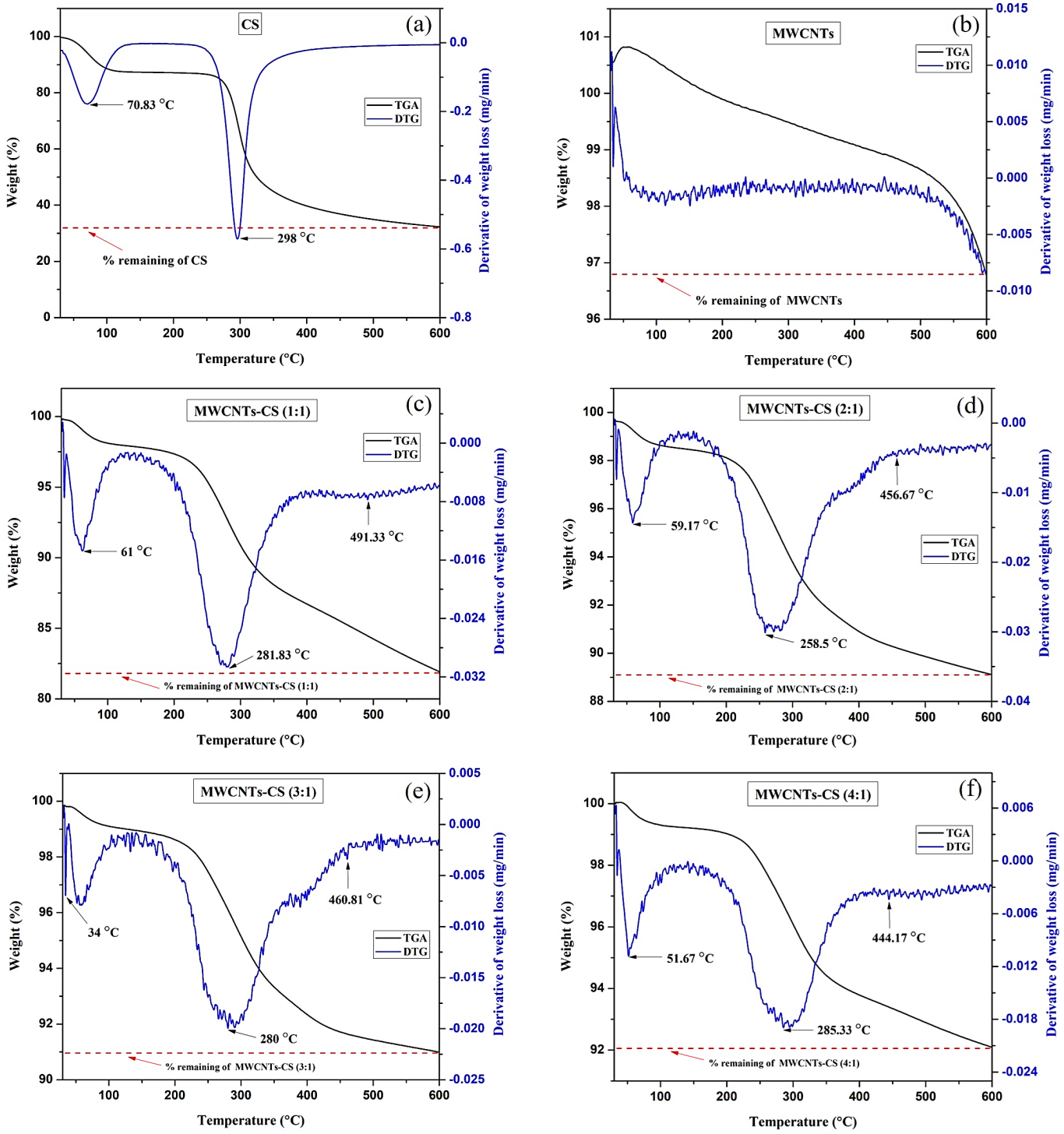


Figure 5. Representative TGA (black curve) and DTG (blue curve) patterns of (a) CS, (b) MWCNTs, (c) MWCNTs-CS (1:1), (d) MWCNTs-CS (2:1), (e) MWCNTs-CS (3:1), and (f) MWCNTs-CS (4:1).

MWCNTs. Additionally, the average size of the pores and the mesopore volume fraction increase with the addition of MWCNTs, which can be attributed to an oxidation-reduction reaction between the oxidation sources in the CS precursor and and so results in enhanced electrochemical performance. In addition, the larger pore size can provide a shorter diffusion route and low resistance pathways for the ions through the porous structure. Large pores are more favorable for ion

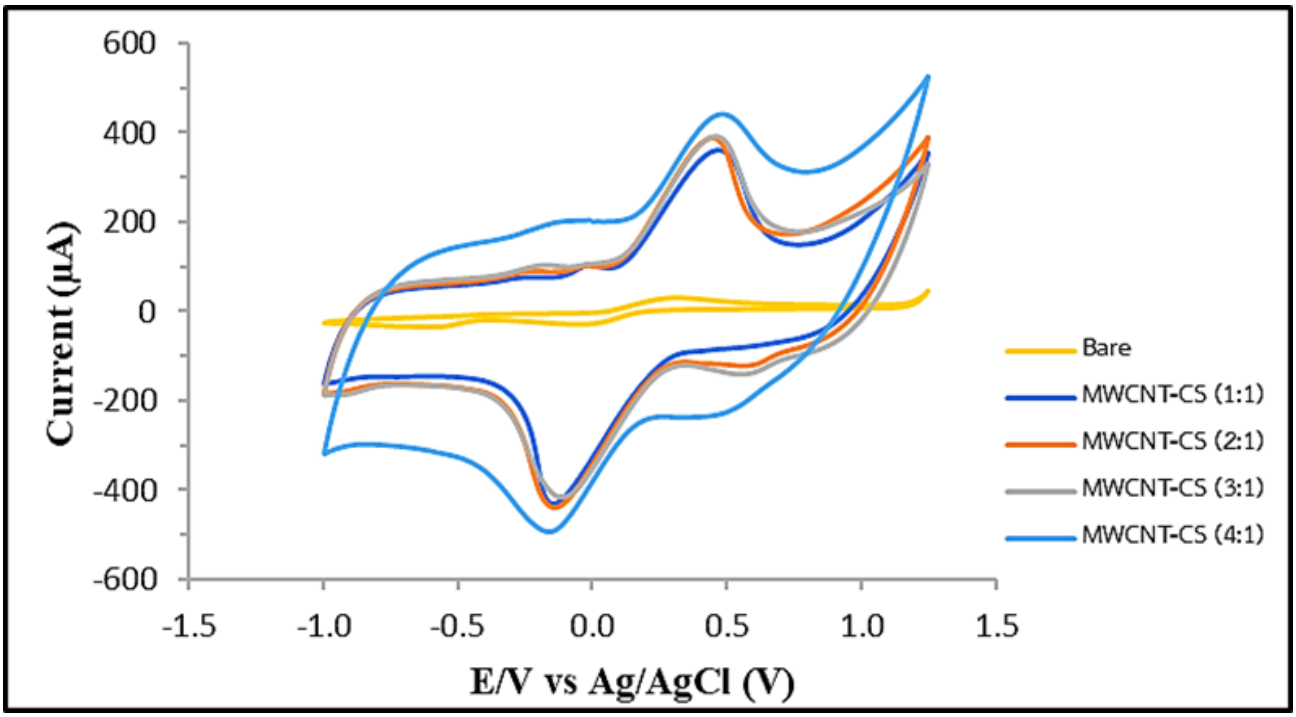


Figure 6. Comparison of the conductivity quality between electrodes modified by MWCNTs-CS composites formed at different MWCNTS: CS ratios compared to bare electrodes using the CV technique over a potential range of -1.0 to 1.25 V at a scan rate of 0.1 V/s in a KCI /$Fe(CN)_3$/$Fe(CN)_2$ solution.

the carbon during the MWCNTs formation process. Notably, the nano-sized MWCNTs-embedded CS exhibit characteristics of high surface area with a large mesopore volume and a high electrical conductivity due to the distribution of the CS phase, diffusion at high speed and current densities based on efficiently utilizing specific surface areas. Accordingly, we examined the electrical and electrochemical properties to investigate the relationship between the porous structure of carbon materials

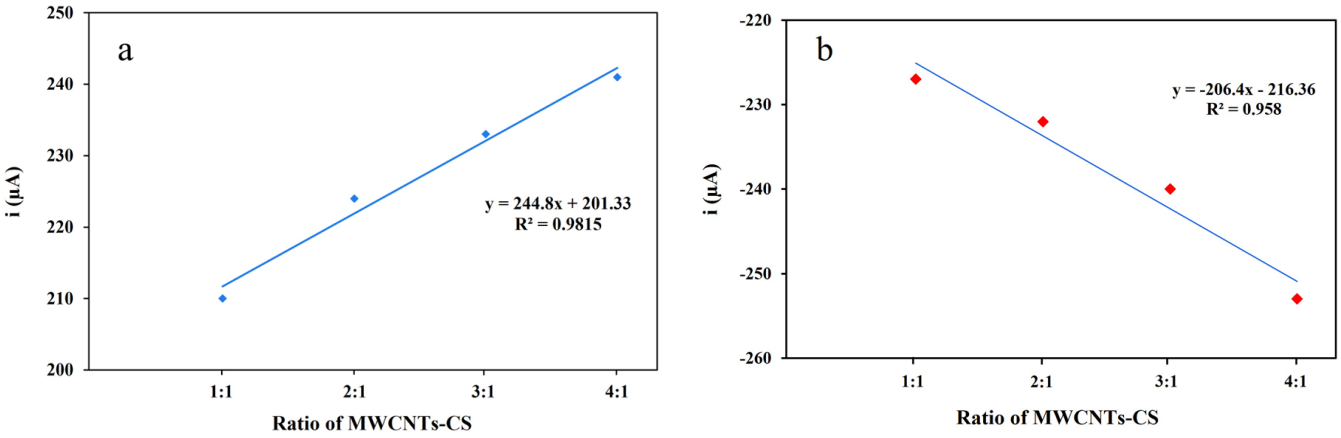


Figure 7. Relationship between the specific conductivity of the MWCNTs: CS ratio of the MWCNTs-CS composite sensor and the obtained (a) oxidation and (b) reduction current obtained in CV with Hcy.

and the electrical conductivity due to the embedding of CS onto the MWCNTs.

3.5. Thermogravimetric analysis

The TGA of CS, MWCNTs, MWCNTs-CS (1:1), MWCNTs-CS (2:1), MWCNTs-CS (3:1), and MWCNTs-CS (4:1) was performed under a 20 mL/min N_2 atmosphere, and its derivatives are shown in Figure 5. As seen, CS has two steps of decomposition, MWCNTs have a single decomposition step, and the MWCNTs-CS (1:1), MWCNTs-CS (2:1), MWCNTs-CS (3:1), and MWCNTs-CS (4:1) composites each have three decomposition steps. For CS (Figure 5a), the first step began at 71 °C up to 110 °C with a weight loss of about 4% to 12%, which was due to dehydration of the saccharide rings and decomposition of the CS, reflecting the hydrophilic nature of CS [24, 25]. The second decomposition step was initiated at around 298 °C due to the depolymerization and decomposition of the basic unit of the polysaccharide polymer [26].

For MWCNTs (Figure 5b), the single-step weight loss at 450– 600 °C was only 3.24%, which shows the thermal stability of the excellent graphite structure of the CNTs [18]. As shown in Figure 5(c-f), MWCNTs-CS (1:1), MWCNTs-CS (2:1), MWCNTs-CS (3:1), and MWCNTs-CS (4:1), each had three decomposition steps with a total weight loss of about 18.09%, 10.89%, 9.01%, and 7.91%, respectively, from 30–600 °C, which is due to the decomposition of CS clustered on the surface of MWCNTs. It also produced a rapid decay at around 280 °C [the DTG curve (blue line) showed a peak at 280 °C], which occurs earlier than the MWCNTs. This is mainly due to the decomposition of the CS surface, which has a decomposition rate similar to that of pure CS. It also indicates that increasing MWCNTs in the composites resulted in a lower decomposition rate. In addition, the residual material weight (as a percentage of the initial weight) of the MWCNTs-CS (1:1), MWCNTs-CS (2:1), MWCNTs-CS (3:1), and MWCNTs-CS (4:1) composites at 600 °C was 81.91, 89.11, 90.99, and 92.09%, respectively, which is in accord with the number of MWCNTs in the composites. Thus, the MWCNTs-CS composites show excellent temperature resistance, establishing that FE-SEM, XRD, Raman, and BET analysis be applied to bioreceptor analysis in the future to examine its characteristics in conjunction with the electrochemical properties.

3.6. Electrocatalytic activity of the MWCNTs-CS working electrode

We next examined the electrochemical properties (by CV analysis) of the MWCNTs-CS electrodes constructed with different MWCNTs-CS ratios. The conductivity quality was comparatively analyzed between the modified MWCNTs-CS and bare electrodes as a control. Potassium chloride with potassium hexacyanoferrate and potassium ferrocyanide solution was used as the electron exchange medium. Significant oxidation-reduction peaks that represent the conductivity of the electrode were observed in the presence of MWCNTs-CS at all concentrations but not with the bare electrode (Figure 6). The highest to the lowest oxidation-reduction peaks found in the MWCNTs-CS composites were those formed at a MWCNTs-CS ratio of 4:1, 3:1, 2:1, and 1:1, respectively. That the highest oxidation-reduction peaks were found at a MWCNTs: CS ratio of 4:1 was attributable to it having the most significant proportion of MWCNTs. As for the MWCNTs-CS formed at other MWCNTs-CS ratios, there was a decreased electric current in accord with the reduced proportion of MWCNTs in the composite. Considering the area of the peak

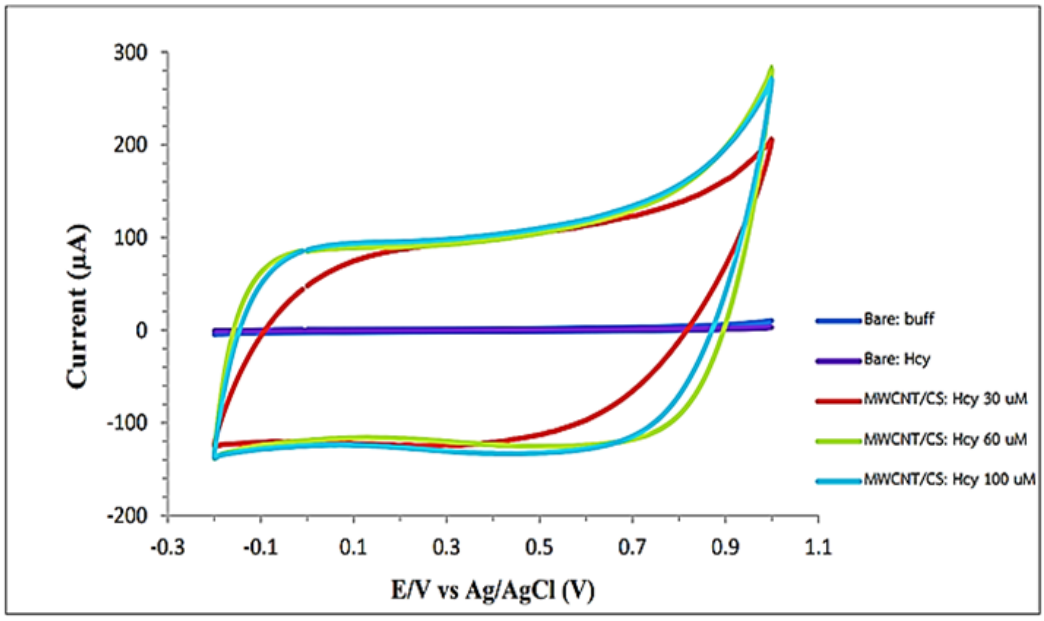


Figure 8. Representative cyclic voltammograms of 30, 60, and 100 µM Hcy solutions using the 4:1 MWCNTs-CS electrode. Conditions: potential range of -0.2 to 1.0 V, scan rate of 0.1 V/s, temperature of 25 °C.

in the MWCNTs-CS composite formed from a 4:1 ratio, the voltage plot has oxidation and reduction peaks at around 0.48 V and -0.16 V, respectively. The measured currents at the oxidation and reduction peaks ranged from 199 to 440 μA and from -239 to -492 μA, respectively—potentially linear relationship between the MWCNTs-CS ratio and the oxidation and reduction peak areas (Figure 6).

Figures 7a and 7b show the relationship between the specific conductivity of MWCNTs-CS (the area of the peak in Figure 6) formed at different composite ratios and their respective oxidation and reduction currents. The current in the oxidation and reduction stages of the 4:1 MWCNTs-CS were highest at 241 μA and -253 μA, respectively. The coefficient of determination (R^2) was 0.9815 and 0.958 in the oxidation and reduction currents, respectively, suggesting a perfectly predictable dependent variable. Therefore, the oxidation current of the 4:1 ratio MWCNTs-CS composite was selected as a subsequent model sensor for Hcy quantification.

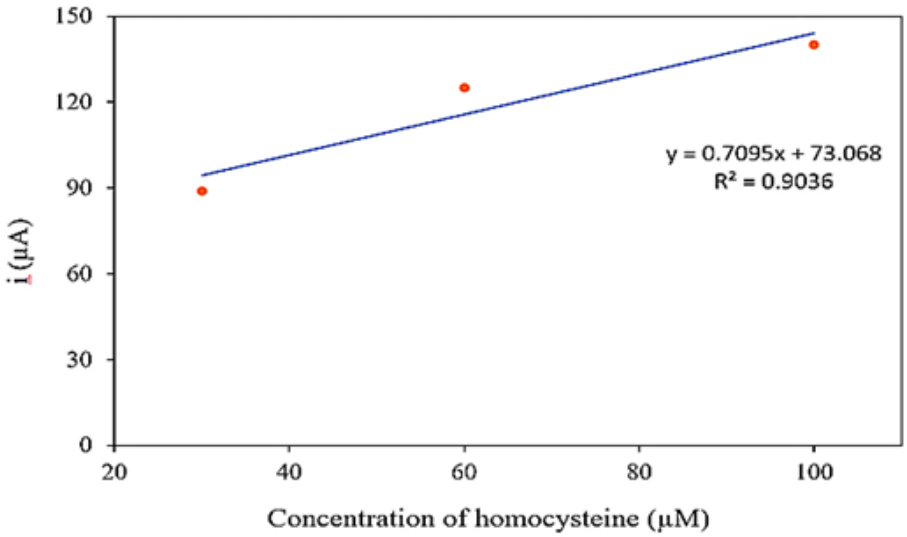


Figure 9. The Hcy concentration-dependence during CV of the current detection using the 4:1 MWCNTs-CS electrode.

3.7. Determination of Hcy levels using the 4:1 MWCNTs-CS coated working SPCE

To further investigate the ability of the 4:1 MWCNTs-CS electrode for Hcy detection, the electrochemical current was measured under different Hcy concentrations. Typically, the normal range of Hcy levels in the blood is less than 15 μM. In contrast, elevated Hcy levels above this level may reflect an increase in the risk of developing atherosclerosis and, thus, CVD. The severity of the risk ranges from mild (at 15–30 μM Hcy) to moderate (30–100 μM) and to severe (> 100 μM) [27]. In order to simulate the human physiologic condition, the present study selected Hcy at concentrations of 30, 60, and 100 μM, comparable to mild, moderate, and severe levels of hyperhomocysteinemia. As for Hcy concentrations below 30 μM, previous research [28, 29] revealed that the observed current values at Hcy concentrations of more than 30 μM exhibited a more excellent direction of measurement, consistent with this work. In contrast, there was a tendency for the measured current to decrease at Hcy concentrations below 30 μM. Therefore, in this work, Hcy concentrations of 30 μM and above were used to reveal the actual risk of CVD. If used in service, an actual Hcy concentration lower than 30 μM will result in a lower measured value by default, indicating a mild to no CVD risk.

As expected, the cyclic voltammograms of the PBS and Hcy in PBS solutions showed no electrochemical oxidation processes with the bare electrode. In contrast, with the 4:1 MWCNTs-CS coated SPCE, the anode current peak corresponded to the Hcy concentrations 4:1 ratio of MWCNTs-CS electrodes in a concentration-dependent manner (Figure 8). The high voltage point in the plot coincides with the oxidation peak of the 30, 60, and 100 μM Hcy solutions at 0.95 V, 0.94 V, and 0.96 V, respectively, with an oxidation current of 89, 125, and 140 μA, respectively.

Little by way of Hcy biosensors exit [10, 17], and those available were developed to screen for Hcy using a carbon paste electrode modified with multiwall carbon nanotubes (MWCNT), and it was used to determine Hcy. The peak current of oxidation of Hcy at MWCNT occurred at a potential of about 0.5–0.7 V. It also showed that the current of the oxidation peak of Hcy at the modified carbon nanotubes electrode was higher than that of the bare electrode, which is in the same direction as our research. However, in our work, the conductivity property was further enhanced for the analytical sensitivity is the electrodes modified with MWCNTs-CS composite. It was found that the oxidation peak current of Hcy, which was altered with the MWCNTs-CS electrode, occurred

at a potential of about 0.9 V and had high measurable current values indicating each level of Hcy that the risk is much. It also shows that the enhanced Hcy measured oxidation peak current has a higher measured current than the bare electrode. This aligns with the work's objectives that highlight the critical levels of risk mentioned above [27].

The coefficient of determination was determined to confirm that the Hcy concentration influenced the oxidation current peaks and a linear relationship between these two factors was found (Figure 9; $R^2 = 0.9036$).

Conclusion

A low-cost and straightforward biosensing method for screening for elevated Hcy levels in human plasma has been developed. The highlight of this study is the production of an innovative formulation to modify MWCNTs with CS, enabling a dramatically increased sensitivity of the biosensor. To validate the microelectrode configuration, it was tested for detecting Hcy. The optimal MWCNTs: CS ratio was found to be 4:1, as confirmed by FESEM, XRD, Raman, BET, and TGA analyses. The CV analysis indicated that the 4:1 MWCNTs-CS electrode could detect the current in the oxidation phase at Hcy concentrations of 30–100 µM ($R^2 = 0.9036$). This promising result is one step closer to creating a disposable biosensor for Hcy monitoring with obvious clinical benefits. Therefore, the researcher now plans to perform a clinical trial and has already applied for registration (ec. number MTU-EC-OO-0-110/65).

Author Contributions

Conceptualization, Suparerk Oonchit, Benya Cherdhirunkorn, Phuntila Tharabenjasin, Noel Pabalan, Yardnapar Parcharoen and Chiravoot Pechyen; Data curation, Benya Cherdhirunkorn, Phuntila Tharabenjasin, Noel Pabalan, Yardnapar Parcharoen and Chiravoot Pechyen; Formal analysis, Suparerk Oonchit, Benya Cherdhirunkorn, Phuntila Tharabenjasin, Noel Pabalan, Yardnapar Parcharoen and Chiravoot Pechyen; Funding acquisition, Yardnapar Parcharoen and Chiravoot Pechyen; Investigation, Suparerk Oonchit, Yardnapar Parcharoen and Chiravoot Pechyen; Methodology, Suparerk Oonchit, Kumpol Chintanavilas, Yardnapar Parcharoen and Chiravoot Pechyen; Project administration, Yardnapar Parcharoen and Chiravoot Pechyen; Resources, Yardnapar Parcharoen and Chiravoot Pechyen; Software, Yardnapar Parcharoen and Chiravoot Pechyen; Supervision, Yardnapar Parcharoen and Chiravoot Pechyen; Validation, Yardnapar Parcharoen and Chiravoot Pechyen; Visualization, Yardnapar Parcharoen and Chiravoot Pechyen; Writing – original draft, Suparerk Oonchit, Yardnapar Parcharoen and Chiravoot Pechyen; Writing – review & editing, Yardnapar Parcharoen and Chiravoot Pechyen.

Funding

This work was funded by the Chulabhorn International College of Medicine Research Fund for giving "General Research Fund Innovation and invention development category of the year 2019" (F1/2562). This work was supported by the Thailand Science Research and Innovation Fundamental Fund fiscal year 2023 (TUFF 27/2566) and Thammasat University Research Fund, Contract No. TUFT 14/2564.

Data Availability Statement

Not applicable

Acknowledgments

The research team thanks the Chulabhorn International College of Medicine Research Fund for the above funding. The Faculty of Science and Technology, Thammasat University, for giving the "Research Promotion Fund Internationalization and Education category of the year 2019".

Conflicts of Interest

The authors declare no conflict of interest. The funders had no role in the design of the study; in the collection, analyses, or interpretation of data; in the writing of the manuscript; or in the decision to publish the results.

References

1. Ageing and health reports for the WHO. https://www.who.int/news-room/fact-sheets/detail/ageing-and-health#, 2022 (accessed 10 October 2022).
2. D. Lorthanavanich, O. Komazawa, Introduction. Population Ageing in Thailand Long-term Care Model: Review of Population Ageing Practices and Policies, 2nd ed.; D. Lorthanavanich, O. Komazawa, Eds.; ERIA: Jakarta: ER-IA, Jakarta, 2021. Volume 2, pp. 1-11.
3. Cardiovascular diseases (CVDs) reports for the WHO. https://www.who.int/news-room/fact-sheets/detail/cardiovascular-diseases-(cvds), 2021 (accessed 12 October 2022).
4. J. Li, J. Zhang, Y. Chen, L. Gao, X. Yan , M. Zhang, F. Wang, Y. He, W. Hu, H. Peng, Mean platelet volume modifies the contribution of homocysteine to cardiovascular disease: A real-world study. 33 (2023) 194-202. https://doi.org/10.1016/j.numecd.2022.10.013
5. G. Paul, F.A. Sreyoshi, Role of homocysteine in the development of cardiovascular disease, Nutrition Journal. 14 (2015) 10. https://doi.org/10.1186/1475-2891-14-6.
6. K. Borowczyk, J. Piechocka, R. Głowacki, I. Dhar, O. Midtun, G. S. Tell, P. M. Ueland, O. Nygård, H. Jakubowski, Urinary excretion of homocysteine thiolactone and the risk of acute myocardial infarction in coronary artery disease patients: the WENBIT trial, J Intern Med. 285 (2019) 232–244.
7. L. Zizhen, H. Qianqian, Y. Hongbo, L. Jiajia, W. Xiaona, Z. Rui, H. Qiuyan, X. Yanchun, L. Guanxian, L. Bin, Y. Qiongqiong, Serum homocysteine is associated with tubular interstitial lesions at the early stage of IgA nephropathy, BMC Nephrology. 23 (2022). https://doi.org/10.1186/s12882-021-02632-3.
8. P. Łukasz, W. Dorota, I. Magdalena, C. Agnieszka, S. Dorota, S. Janusz, Analysis of serum homocysteine

in the laboratory practice - comparison of the direct chemiluminescence immunoassay and high performance liquid chromatography coupled with fluorescent detection, Biochem Med (Zagreb). 30 (2020) 030703.
9. F.A. Sreyoshi, K. Santosh, G. Paul, Measurement of homocysteine: a historical perspective, J Clin Biochem Nutr. 65 (2019) 171–177. doi: 10.3164/jcbn.19-49.
10. M. Safoora, F. Masoud, Electrocatalytic oxidation and determination of homocysteine at nanotubes-modified carbon paste electrode using dopamine as a mediator, J. Serb. Chem. Soc. 78 (2013) 1595–1607. doi: 10.2298/JSC1210 19022M.
11. S. Yichi, F.H. Scott, G.L.K. Samantha, C.H. Ming, In Vitro and In Vivo Enzyme Activity Screening via RNA-Based Fluorescent Biosensors for S-Adenosyl-l-homocysteine (SAH), Journal of the American Chemical Society. 138 (2016) 7040-7047. https://doi.org/10.1021/jacs.6b01621.
12. A. Assareeya, C. Benya, P. Chiravoot, Development of screen printed electrode using MWCNTs–TiO_2 nanocomposite as a low-cost device for uric acid detection in urine, Journal of Materials Science: Materials in Electronics. 30 (2019) 2403–2412. https://doi.org/10.1007/s10854-018-0513-z.
13. N. Hui-Bog, R. S. Brillians, S. Yoon-Bo, Voltammetric analysis of anti-arthritis drug, ascorbic acid, tyrosine, and uric acid using a graphene decorated-functionalized conductive polymer electrode, Electrochimica Acta. 139 (2014) 315-322. https://doi.org/10.1016/j.electacta.2014.07.044.
14. T.E.M. Nancy, V.A. Kumary, Synergistic electrocatalytic effect of graphene/nickel hydroxide composite for the simultaneous electrochemical determination of ascorbic acid, dopamine and uric acid, Electrochimica Acta. 133 (2014) 233-240. https://doi.org/10.1016/j.electacta.2014.04.027.
15. R. Mahmoud, S. Mojtaba, R.R. Hamid, Highly selective detection of dopamine in the presence of ascorbic acid and uric acid using thioglycolic acid capped CdTe quantum dots modified electrode, Journal of Electroanalytical Chemistry. 712 (2014) 19-24. https://doi.org/10.1016/j.jelechem.2013.08.027.
16. B.F. Sekli, A. Civélas, V. Castagnola, A. Tsopela, L. Mazenq, P. Gros, J. Launay, P. Temple-Boyer, PEDOT-modified integrated microelectrodes for the detection of ascorbic acid, dopamine and uric acid, Sens. Actuators B. 214 (2015) 1-9. https://doi.org/10.1016/j.snb.2015.03.005.
17. M. Fouladgar, S. Mohammadzadeh, H. Nayeri, Electrochemical determination of homocysteine using carbon nanotubes modified paste electrode and isoprenaline as a mediator, Russian Journal of Electrochemistry. 50, (2014) 981–988.
18. M. Debasis, M. Mathankumar, T.R.K. Ramasamy, Development of the PANI/MWCNT nanocomposite-based fluorescent sensor for selective detection of aqueous ammonia, ACS Omega. 5 (2020) 8414–8422. https://dx.doi.org/10.1021/acsomega.9b02885.
19. B.A. Shujahadeen, M. H. Hamsan, M. F. Z. Kadir, H. J. Woo, Design of Polymer Blends Based on Chitosan:POZ with Improved Dielectric Constant for Application in Polymer Electrolytes and Flexible Electronics, Advances in Polymer Technology, (2020) 10. https://doi.org/10.1155/2020/8586136.
20. K. Divya, R. Sharrel, S. Jisha, A simple and effective method for extraction of high purity chitosan from shrimp shell waste, International Conference on Advanced Applied Science Environment Engineering. (2014) 140-145.
21. X. S. Zhang, L. W. Yang, H. T. Liu, M. Zu, A novel high-content CNT-reinforced SiC matrix composite-fiber by precursor infiltration and pyrolysis process, RSC Adv. 7 (2017) 23334-23341. doi: 10.1039/C7RA03339G.
22. A. Tamilselvan, K. Ganapathy, R. Ramasamy, B. Sengottuvelan, Antifouling behavior of chitosan adorned zinc oxide nanorods, RSC Adv. 6 (2016) 69206-69217. doi: 10.1039/c6ra13321e.
23. V. Damini, C. Deepika, D.M. Maumita, R.R. Kumar, Y. Amit K, S. Pratima R, Development of MWCNT decorated with green synthesized AgNps-based electrochemical sensor for highly sensitive detection of BPA, Journal of Applied Electrochemistry. 51 (2021) 447-462.
24. N. Laura, M. A. Journot. Céline, G.L. Sandrine, Chitosan functionalization: covalent and non-covalent interactions and their characterization, Polymers. 13 (2021) 4118. https://doi.org/10.3390/polym13234118.
25. C.D. Shaikat, A.A. Mohammad, U.R. Taslim, M.S. Zakir, M. Ashaduzzaman, S. Mithun, Sayed M. Shamsuddin, Preparation, characterization and performance evaluation of chitosan as an adsorbent for Remazol red, International Journal of Latest Research in Engineering and Technology. 2 (2016) 52-62.
26. N.A. Rahman, S. Abu. Hanifah, N.N. Mobarak, M.S. Su'ait, A. Ahmad, L.K. Shyuan, L.T. Khoon, Synthesis and characterizations of o-nitrochitosan based biopolymer electrolyte for electrochemical devices. Europe PMC. 14 (2019).
27. B. Hadi, Z. Reza, T.M. Masoud, T. Somayeh, A label-free aptasensor for highly sensitive detection of homocysteine based on gold nanoparticles, Bioelectrochemistry. 134 (2020) 107497. https://doi.org/10.1016/j.bioelechem.2020. 107497.
28. Z. Reza, T. Somayeh, B. Hadi, T.M. Masoud, Fabrication of a novel and ultrasensitive label-free electrochemical aptasensor based on gold nanostructure for detection of homocysteine, Biosensors 13 (2023) 244. https://doi.org/10.3390/bios13020244.
29. H. Laleh, K. Alireza, A. Kourosh, R.N. Mehdi, A. Farhad, Determination of homocysteine using a dopamine-functionalized graphene composite, Microchemical Journal. 165 (2021) 106124. https://doi.org/10.1016/j.microc. 2021.106124.